

A&A manuscript no.

(will be inserted by hand later)

Your thesaurus codes are:

04(11.09.1 Dw1, 11.09.1 Dw2, 11.09.03, 11.11.1, 11.12.1, 11.19.2)

ASTRONOMY  
AND  
ASTROPHYSICS  
28.3.2022

# Neutral hydrogen in the nearby galaxies Dwingeloo 1 and Dwingeloo 2

W.B. Burton<sup>1</sup>, M.A.W. Verheijen<sup>2</sup>, R.C. Kraan–Korteweg<sup>2,3</sup>, and P.A. Henning<sup>4</sup>

<sup>1</sup> Sterrewacht Leiden, Postbus 9513, 2300 RA, Leiden, The Netherlands

<sup>2</sup> Kapteyn Astronomical Institute, Postbus 800, 9700 AV, Groningen, The Netherlands

<sup>3</sup> Observatoire de Paris–Meudon, DAEC, 5 Place Jules Janssen, F-92195 Meudon–Cedex, France

<sup>4</sup> Department of Physics and Astronomy, University of New Mexico, Albuquerque, NM 87801, U.S.A.

Received ..., 1995; accepted ..., 1995

**Abstract.** We present observations made with the Westerbork Synthesis Radio Telescope of HI emission from Dwingeloo 1, a nearby barred spiral discovered during the Dwingeloo Obscured Galaxies Survey for galaxies hidden in the Zone of Avoidance, and of Dwingeloo 2, a small galaxy discovered in the beam of these WSRT observations. The WSRT data reveal the position of the dynamical center of Dw1, its systemic *LSR* velocity, its total (projected) width in velocity, its inclination on the sky, and its integrated HI flux, as well as details of the velocity field and gas distribution. Dw1 is the nearest grand-design barred spiral system, and is probably amongst the ten largest galaxies closer than about 5 Mpc. We report here also the discovery of Dwingeloo 2, a small galaxy located within the WSRT primary beam as pointed to Dw1. In view of its angular and kinematic proximity to Dw1, Dw2 may well be a companion to the larger system. The two galaxies are probably both members of the group containing Maffei 1 & 2 and IC342 and may influence the peculiar motions within that group and the morphology of its individual members.

**Key words:** galaxies: individual: Dw1 – galaxies: individual: Dw2 – galaxies: interstellar medium – galaxies: spiral – galaxies: kinematics and dynamics – galaxies: Local Group

incomplete closer than about  $5^\circ$  to the galactic equator, where the optical and infrared sky is grossly confused by local stars and other objects and where deep optical searches for obscured galaxies fail (see Kraan–Korteweg & Woudt, 1994). The boundaries of the Zone of Avoidance are difficult to quantify; there are patches of sky beyond  $|b| \sim 5^\circ$  where the optical depth is also substantial. The intervening interstellar medium which is largely opaque at optical wavelengths is transparent at the 21-cm wavelength of neutral hydrogen. Reviews of the use of the HI line to search for galaxies in the Zone of Avoidance have been given by Kerr and Henning (1987), by Kerr (1994), and by Henning (1992, 1994).

The Dwingeloo Obscured Galaxies Survey has been searching for HI emission from galaxies hidden behind the obscuring material causing the Zone of Avoidance, using the 25-m radio telescope of the Netherlands Foundation for Research in Astronomy, located in Dwingeloo. The project is motivated by the hope to find the HI signatures of fairly nearby galaxies in the velocity range  $0 - 4000 \text{ km s}^{-1}$ . Such detections would contribute to investigations of the dynamics of the Local Group, of the morphological distribution of nearby galaxies, of the age of the Universe as determined by the timing argument, and of the density parameter  $\Omega$  as revealed by the velocity of the Local Group relative to the Microwave Background.

It is expected that the Dwingeloo Obscured Galaxies Survey will continue, utilizing the telescope essentially full-time, for a duration of several years. Before this search began, the Dwingeloo 25-m telescope had been used over a five-year period to produce the Leiden/Dwingeloo atlas of HI in our Galaxy over the entire sky at  $\delta > -30^\circ$  and within the velocity range  $-450 < v < +400 \text{ km s}^{-1}$  (Hartmann, 1994; Hartmann & Burton, 1995). That survey represented the first use of the 25-m telescope with the new *DAS* 1000-channel digital autocorrelator spectrometer combined with the receiver, characterized by a system

## 1. Introduction; the Dwingeloo Obscured Galaxies Survey

Some 20% of the optical sky is significantly obscured by absorption and scattering of light by intervening interstellar material in the Milky Way. As a consequence of this obscuration, the inventory of nearby galaxies is certainly

*Send offprint requests to:* W.B. Burton

**Fig. 1.** Mosaic of channel maps showing the H I emission from Dwingeloo 1, after subtraction of the 21-cm continuum radiation and after application of the *CLEAN* algorithm, but uncorrected for primary-beam attenuation. For each panel the appropriate central *LSR* velocity is indicated; the cross indicates the position of the dynamical center. The ellipse in the upper-left-hand panel indicates the approximate size and orientation of the optical image obtained with the Isaac Newton Telescope in the *I*-band image (see Loan et al. 1995). Contour lines in the channel maps correspond to  $-0.42, -0.21, 0.21$  (the  $2\text{-}\sigma$  level),  $0.42, 0.85, 1.3, 1.7, 2.5, 3.4,$  and  $4.2 \times 10^{20}$  H I atoms  $\text{cm}^{-2}$ . The first five channel maps show contaminating H I emission from our own Galaxy. The lower-right-hand panel shows the (un-*CLEAN*ed) continuum radiation from the field, for which the individual channel maps have been corrected. Contour lines in this continuum map correspond to  $-1.3, -0.62, 0.62$  (the  $2\text{-}\sigma$  level),  $1.3, 2.5, 5.0, 7.5, 10, 13,$  and  $15$  K; dashed-line contours represent the negative values.

temperature of about 35 K, which is a prototype of the sort mounted on the telescopes of the Westerbork array. The experience gained with the Leiden/Dwingeloo Milky Way survey confirmed that the interference environment was benign enough, and the telescope electronics stable and sensitive enough, to justify the search for obscured, relatively nearby, galaxies.

The performance and operating configuration of the Dwingeloo 25-m telescope currently pertaining is that described by Hartmann (1994), Burton & Hartmann (1994), and Hartmann & Burton (1995). For the obscured-galaxies project, the radio receiver is tuned to a central frequency corresponding to a velocity of  $+2000$   $\text{km s}^{-1}$  above the rest frequency of the H I hyperfine transition; the bandwidth of the 1000-channel spectrometer is set to cover the range  $0 < v < +4000$   $\text{km s}^{-1}$  at  $4$   $\text{km s}^{-1}$  resolution. (Radial velocities are defined here following the radio convention and are referred to the Local Standard of Rest defined by the Standard Solar Motion of  $20$   $\text{km s}^{-1}$  towards  $\alpha, \delta = 18^{\text{h}}, +30^{\circ}$ , epoch 1900.)

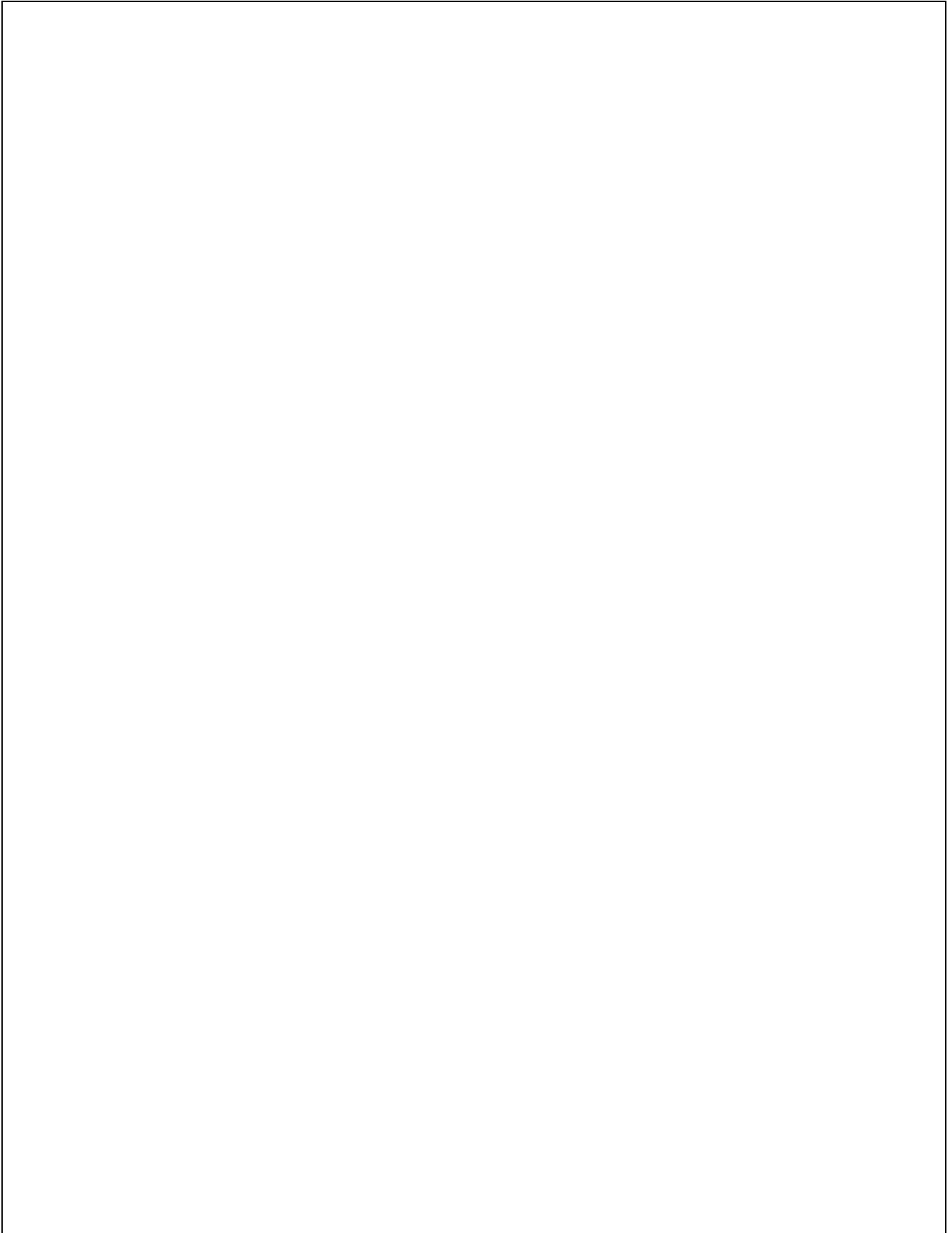
The Dwingeloo Obscured Galaxies Survey involves a strategy with several different facets. Two blind searches will fully sample the Zone of Avoidance; first, a program of short (5-minute) integrations has been searching for H I emission from large, or particularly nearby, hidden galaxies; a program of longer ( $12 \times 5$ -minutes) observations has now been initiated looking for smaller, or more distant systems. Both blind searches involve observing on a honeycomb grid with lattice points separated by  $0^{\circ}35'$ ; because the FWHM beam of the 25-m telescope operating at a wavelength of 21 cm is 36 arcminutes, the honeycomb grid is fully sampling the beam. The blind searches are covering the regions of full optical obscuration at  $|b| < 5^{\circ}$ , over most of the accessible range in longitude. The initial period of the survey has been directed toward the longitude range in the second quadrant where the Supergalactic equator crosses the Zone of Avoidance and where a large population of galaxies is expected a priori. (Most of the galaxies – all of them previously known ones – identified as contaminating nuisances in the Leiden/Dwingeloo survey of H I in the Milky Way occur in a vertical swath crossing the equator of the Milky Way near the center of the second longitude quadrant: see e.g. figure 4.4 in Hartmann, 1994, or figure 5 in Burton & Hartmann, 1994.) Although the blind searches are the principal facets of the strategy,

a limited directed search is being carried out involving longer integrations toward candidate objects selected from optical and infrared datasets. Integration times of an hour per spectrum yield sensitivities of about 0.01 K over the range  $0 < v < +4000$   $\text{km s}^{-1}$ .

Many problems can plague single-dish 21-cm spectra. In particular, the expected emission signature of an external galaxy can be mimicked by interference signals of unusual type, i.e. not appearing as a single-channel spike or as a  $\sin(x)/x$  ringing (see figure 2.13 of Hartmann, 1994); the signal from a low-velocity galaxy like either Dw1 or Dw2, or like Maffei 2, might be at least partly blended with that from conventionally-behaving gas associated with the Milky Way, or it might resemble that of a (very) high-velocity cloud associated with the Milky Way; the signal might be confused with edge-of-bandpass effects; or the signal might be contaminated by enhanced system temperatures due to the appearance of a Milky Way H II region, a plethora of which occur at the latitudes being searched (see e.g. Lockman’s 1989 catalog). Each of these problems could be dealt with at the 25-meter telescope itself, but an important aspect of the strategy of the Dwingeloo Obscured Galaxies Survey is the intention to seek rapid independent confirmation of suspected detections by using the Westerbork Synthesis Radio Telescope in the “snapshot” mode. Thus the detection spectrum of Dwingeloo 1 (see Kraan–Korteweg et al., 1994) was discussed amongst members of the project team in a meeting in Dwingeloo on Thursday, August 4, 1994, and by the end of the day on Monday, August 8, a WSRT snapshot was in hand confirming the detection and giving preliminary information on the H I position and flux. By the end of that week, optical and near- as well as far-infrared identifications of the newly detected galaxy had also been obtained (see Kraan–Korteweg et al. 1994; Loan et al. 1995). We discuss here full  $4 \times 12$  hour synthesis observations of Dwingeloo 1, and the discovery in these observations of another galaxy, which we call Dwingeloo 2 and which is probably a companion to Dw1.

## 2. WSRT observing program

The Westerbork Synthesis Radio Telescope is an interferometer comprising an array of 14 telescopes, each with a diameter of 25 meters. The east-west alignment implies



that the technique of earth-rotation aperture synthesis requires an observation of 12 hours duration to obtain a synthesized field. The observations reported here were carried out in five sessions during August and September, 1994, and resulted in a full synthesis of  $4.4 \times 12$  hours duration, including the snapshot material. The four eastern, movable telescopes were set at different positions during the different 12-hour periods, and the signals from the fixed-movable telescope pairs were correlated; this provided a total of 152 different baselines ranging in length from 36 to 2754 meters with a standard increment of 18 meters. As a result, the instrumental grating rings caused by the constant increment in baseline length lie well beyond the FWHM of the primary beam and do not interfere with extended emission.

The synthesized beam has an elliptical shape with dimensions  $\alpha \times \delta = 11.8 \times 13.8$  arcsec. The FWHM size of the primary beam of the WSRT when operated at a wavelength of 21 cm is 37.6, quite similar to that of the single-dish Dwingeloo telescope. A series of spectra made with the 25-m telescope at neighboring pointings around the source later to be identified as Dwingeloo 1 had given a rough indication of the direction towards which the WSRT should be pointed for the initial “snapshot” observation, and the suspicion (correct, as it turned out) that the smudge on the red Palomar Sky Survey plate (#936) catalogued by Hau et al. (1995) might be the counterpart to the HI feature, led to centering the WSRT on the direction  $\alpha = 02^h 53^m 02^s$ ,  $\delta = +58^\circ 42' 36''$  (epoch 1950). The central frequencies of the WSRT receivers were tuned to correspond to an *LSR* velocity of  $106 \text{ km s}^{-1}$ . The single-dish detection had shown the double-horned signature characteristic of HI emission from a spiral galaxy, but the extent to which the lower-velocity horn was contaminated by emission from the Milky Way was not clear until the WSRT data confirmed that the central-frequency tuning of the receivers was reasonably accurate. A total bandwidth of 2.5 MHz was covered by 63 channels; during the observations an on-line uniform frequency taper was applied, yielding a velocity resolution of  $9.89 \text{ km s}^{-1}$ .

The interferometric *UV*-plane data were calibrated, flagged if necessary, and Fourier transformed with the *NEWSTAR* software package. Before Fourier transforming, the *UV*-plane data were convolved with an *expsinc* function to reduce aliasing effects, and a Gaussian baseline taper was applied to suppress the sidelobes of the synthesized beam. Furthermore, the *UV*-data were weighted according to the local density of data points in the *UV*-plane. Due to decreasing sensitivity near the edges of the bandpass, the first 3 as well as the last 7 channels were discarded. This procedure resulted in a data cube containing  $1024 \times 1024 \times 53$  pixels, covering a field of angular dimensions  $1^\circ 42' \times 1^\circ 66'$  with a synthesized beam of FWHM of  $11''.8$  in  $\alpha$  and  $13''.8$  in  $\delta$ . The total velocity coverage was  $428.7 \text{ km s}^{-1}$ . Application of the various tapers and convolution functions yielded an rms noise in the channel

**Table 1.** Westerbork observing parameters for the Dwingeloo 1 field

field center (1950.0)	$\alpha$	$02^h 53^m 02^s$
	$\delta$	$58^\circ 42' 36''$
dates of observations		8 & 12 Aug. 1994 6, 26 & 29 Sept. 1994
length of observations		$4.4 \times 12$ hours
number of different baselines		152
baselines (min–max–incr)		36–2754–18 meters
FWHM of synthesized beam ( $\alpha \times \delta$ )		$11.8 \times 13.8$ arcsec
radius of first grating ring ( $\alpha \times \delta$ )		$40.1 \times 47.0$ arcmin
FWHM of primary beam		37.6 arcmin
rms noise in one channel map		4.8 K
central frequency		1420.01 MHz
central velocity ( <i>LSR</i> )		$106 \text{ km s}^{-1}$
bandwidth		2.5 MHz
number of channels		63
channel separation		$8.24 \text{ km s}^{-1}$
velocity resolution		$9.89 \text{ km s}^{-1}$
K $\Rightarrow$ mJy conversion, equivalent of 1 mJy/beam		4.24 K

maps of 1.2 mJy per beam. A set of 5 maps with the antenna patterns at different frequencies was constructed for use when applying the *CLEAN* algorithm to the channel maps.

Further reduction and analysis of the data utilized the Groningen Image Processing SYstem (*GIPSY*), following practices described by Verheijen (1996). First, the data cube was smoothed to spatial resolutions of 30 and 60 arcseconds in order to obtain higher sensitivity to extended emission at low column densities. These smoothed data cubes showed that HI emission from Dw1 covers the velocity interval extending from 7 to  $221 \text{ km s}^{-1}$ ; the emission from Dw2 extends from 32 to  $156 \text{ km s}^{-1}$ . Because the channels at velocities below about  $25 \text{ km s}^{-1}$  are contaminated by HI emission from the Milky Way, a map of the 21-cm *continuum* emission was made by averaging 10 channels at velocities from 229.7 to  $303.9 \text{ km s}^{-1}$ , which were judged to be free of any HI emission either from the Milky Way or from the galaxies in question. The rms noise in the resulting high-resolution continuum map is 0.37 mJy/beam. The continuum map was subtracted from each channel map in the data cube. The continuum-subtracted channel maps which do contain HI emission from Dw1 and Dw2, as well as the continuum map itself, were *CLEANed* by applying that algorithm in the standard manner (see Högbom 1974). The map areas to be cleaned were determined by the  $2\text{-}\sigma$  contour in the un-*CLEANed* map at  $60'' \times 60''$  resolution and extended by 1 arcmin in order to account for possible emission suppressed by the sidelobes below the formal  $2\text{-}\sigma$  level. Note that these areas vary from channel to channel due to the rotation of both galaxies. The selected areas were *CLEANed* down to the  $0.3\text{-}\sigma$

**Fig. 2.** Global kinematic and spatial properties of the H I distribution in Dwingeloo 1. Panel *a*) shows, for comparison with the global H I situation, a greyscale representation of the INT *I*-band image (see Loan et al. 1995). The size and orientation of the optical image is represented by the ellipse in panel *b*), which shows the *CLEAN*ed continuum map, with contours drawn at levels of  $-1.2$ ,  $-0.58$ ,  $0.58$  (the  $2\text{-}\sigma$  level),  $1.2$ ,  $2.3$ ,  $4.6$ ,  $9.3$ , and  $19$  K. Panel *c*) shows the global H I line profile in mJy, corrected for the sensitivity of the primary beam; the vertical arrow shows the systemic velocity of Dw1,  $110.3$  km s $^{-1}$ , as derived from the velocity-field data. Panel *d*) shows the deprojected H I surface density in units of  $M_{\odot}$  pc $^{-2}$ , as determined in tilted, rotating rings separately for the approaching and receding sides of Dw1; the full-drawn line corresponds to the average of the surface densities measured on the two sides; the vertical arrow shows the angular extent of the semi-major axis of the optical image. The panels labelled *e*) show position-velocity maps of the H I emission observed, at the indicated position angles, along the kinematic major axis (left) and along the kinematic minor axis (right) of Dw1. Contours in the major-axis position-velocity map correspond to  $-0.36$ ,  $-0.18$  (the  $2\text{-}\sigma$  level),  $0.18$ ,  $0.36$ ,  $0.73$ ,  $1.1$ ,  $1.5$ ,  $2.2$ ,  $2.9$ , and  $3.6 \times 10^{20}$  H I atoms cm $^{-2}$ ; in the minor-axis map, the contours correspond to  $-0.42$ ,  $-0.21$ ,  $0.21$  ( $2\sigma$ ),  $0.42$ ,  $0.85$ ,  $1.3$ ,  $1.7$ ,  $2.5$ , and  $3.4 \times 10^{20}$  H I atoms cm $^{-2}$ . The dots follow the rotation curve as projected onto this position-velocity maps. In both panels, the horizontal dashed line gives the systemic velocity while the vertical one corresponds to the location of the center of rotation; the Milky Way contributes the emission contaminating the lower-velocity portion of each of these panels. The cross in the lower-left hand corner of each of the position-velocity slices gives the spatial and kinematic resolution of the WSRT data. Panel *g*) shows the observed velocity field determined for Dw1 by Gaussian fitting to individual H I spectra. The lighter greyscale and the black contours correspond to the approaching side; the darker greyscale and the white contours, to the receding. The heavily-drawn black contour follows the systemic velocity. The interval between contour lines is  $20$  km s $^{-1}$ , measured from the systemic velocity of  $110.3$  km s $^{-1}$ . Panel *i*) shows the modelled velocity field as a “spider diagram” derived by fitting the observed field with tilted rings in which the H I describes circular rotation; the isovelocity contours in this panel are drawn as in *g*). Panel *j*) shows the difference between the observed and modelled velocity fields; the contours give the velocity residuals at levels of  $-10$ ,  $-5$ ,  $5$ , and  $10$  km s $^{-1}$ . Panel *h*) shows the distribution of the total H I column density across Dw1. As indicated in the text, the noise level varies across this map. Greyscaled pixels in the total-H I map all have a signal-to-noise ratio  $\geq 1.5$ ; the contours correspond to  $1.8$  (mean  $S/N = 3$ ),  $3.0$ ,  $6.1$ ,  $9.1$ ,  $12$ , and  $18 \times 10^{20}$  H I atoms cm $^{-2}$ . The three panels in *f*) show the radial variations of, respectively beginning with the upper of the three, the inclination of tilted rings fit to Dw1, the position angle of these rings, and the rotation velocity. The rotation velocity was determined separately for the approaching and receding sides, as indicated. The full-drawn line in the rotation-curve panel does not correspond to the average of these two solutions, but to a separate solution incorporating complete rings. The filled circle in the two upper panels and in the one on the lower left indicates the FWHM of the synthesized WSRT beam.

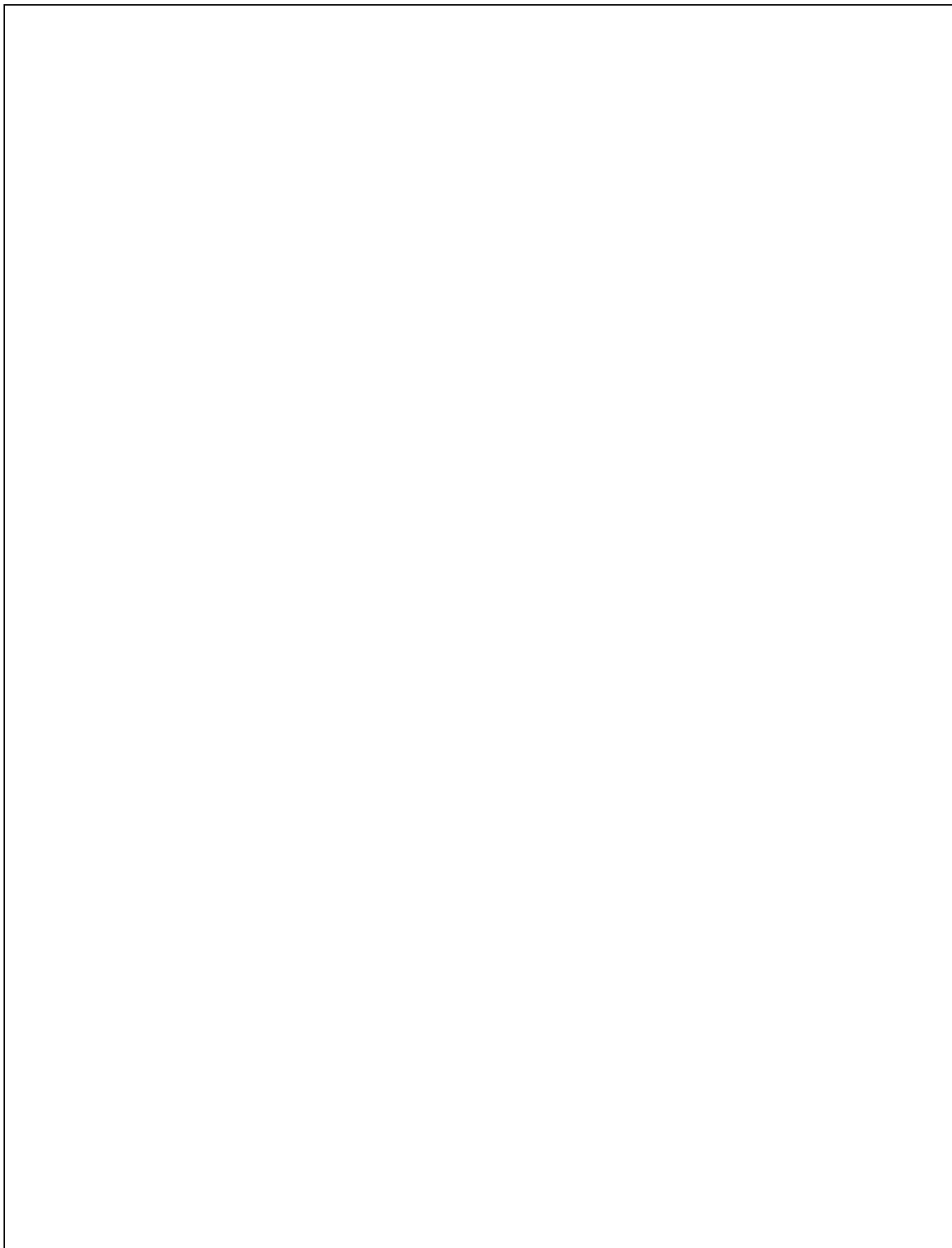
level. The *CLEAN* components were restored by Gaussian beams of FWHM dimensions  $11'' \times 13''$ ,  $30'' \times 30''$ , and  $60'' \times 60''$ , respectively. The rms noise in the continuum-subtracted and *CLEAN*ed channel maps is  $1.2$ ,  $1.6$ , and  $2.3$  mJy/beam for the maps at high, medium, and low resolutions, respectively. After *CLEAN*ing, the map areas containing H I emission were redefined on the basis of the  $2\text{-}\sigma$  level in the *CLEAN*ed maps at  $60'' \times 60''$  resolution. The maps at  $30'' \times 30''$  resolution give the best compromise between resolution and sensitivity and are thus the ones considered further here.

The global H I profiles of Dw1 and Dw2 were determined by summation of the total signal, primary-beam-corrected, in those areas. Taking the primary beam attenuation into account, the sum of the two global H I profiles, one for Dw1 and one for Dw2, corresponds very well to the single-dish detection spectrum measured toward Dw1 on the Dwingeloo 25-m telescope by Kraan–Korteweg et al. (1994), as well as with the spectrum observed subsequently by Huchtmeier et al. (1995) using the Effelsberg 100-m telescope .

Relevant parameters of the WSRT observing program are summarized in Table 1.

### 3. H I in Dwingeloo 1

Fig. 1 is a mosaic of channel maps showing the H I emission from Dwingeloo 1; the panels represent alternate channels, each corresponding to the emission over an interval  $8.2$  km s $^{-1}$  wide centered at the indicated velocity. The first five panels in the series show contamination from H I emission from the Milky Way. The last panel shows the subtracted continuum map. H I emission from Dw1 is evident in each of the displayed panels representing channels centered between  $15$  and  $213$  km s $^{-1}$ . The emission shows the “spider-diagram” isovelocity characteristics which are the signature of H I in an inclined spiral galaxy. The ellipse drawn in the upper-left hand panel of Fig. 1 represents schematically the orientation and size of the optical image of Dw1 observed in the *I*-band with the Isaac Newton Telescope on La Palma (see Kraan–Korteweg et al. 1995; Loan et al. 1995); the image itself is reproduced in Fig. 2a. The spatial extent of the Dw1 H I channel-map slices is clearly larger than the extent of the optical-image ellipse. Although such a situation is common for spiral galaxies, we note that the optical obscuration at  $b = -0^{\circ}11$  is so severe that the outer boundary of the *I*-band image is probably not a quantitative measure of the actual extended stellar dimensions of the system.



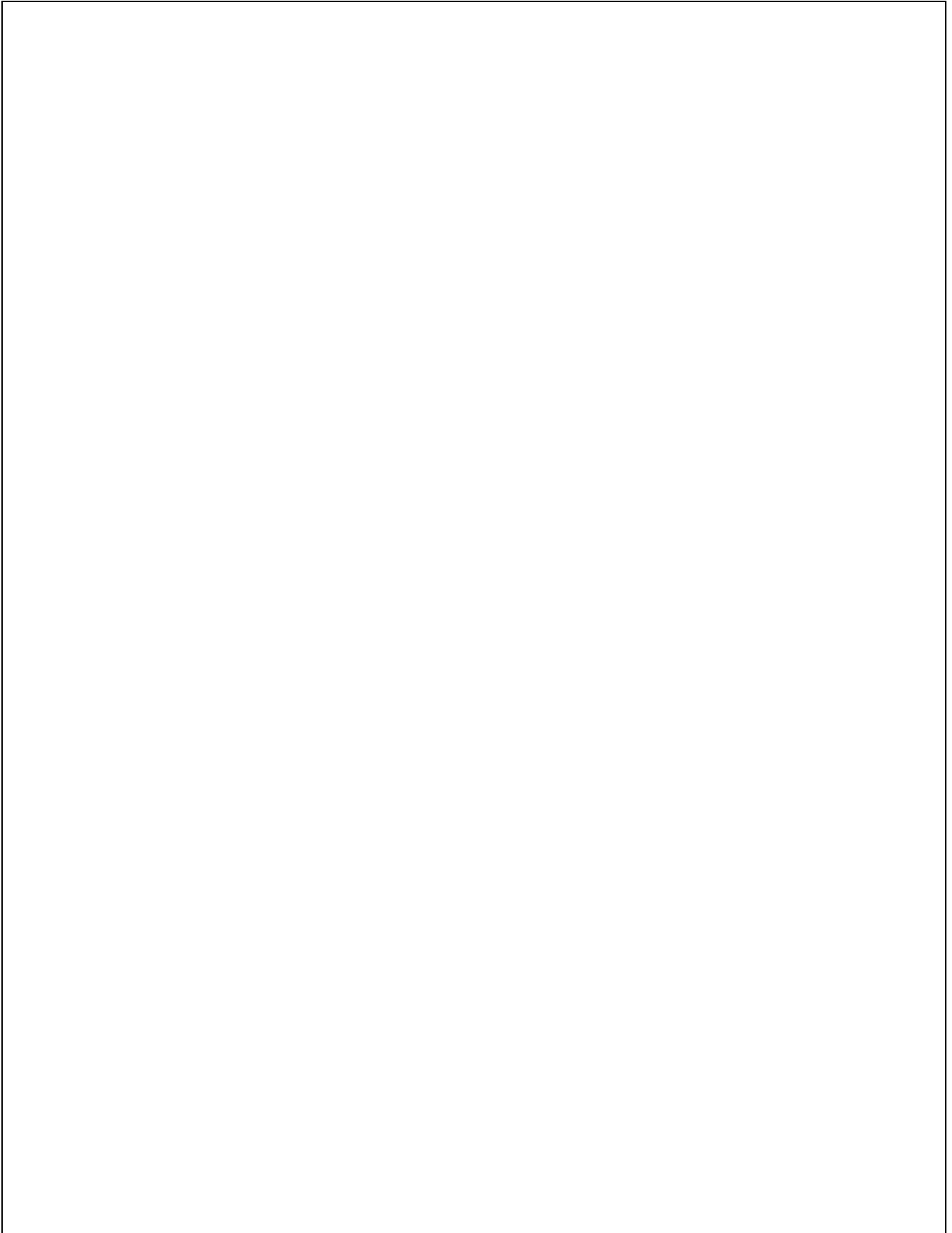


**Fig. 3.** Mosaic of channel maps showing the HI emission from Dwingeloo 2, after subtraction of the background continuum radiation and after application of the *CLEAN* algorithm, but uncorrected for primary-beam attenuation. For each channel map the appropriate central *LSR* velocity is separately indicated; a cross indicates the position of the dynamical center. The lower-righthand panel shows the (un-*CLEAN*ed) continuum radiation from the field, which was subtracted from the individual channel maps. Contour lines in the channel maps are drawn as in Figure 1. Contour lines in the continuum map correspond to  $-1.3$ ,  $-0.62$ ,  $0.62$  (the  $2\text{-}\sigma$  level),  $1.3$ ,  $2.5$ ,  $5.0$ ,  $7.5$ ,  $10$ ,  $13$ , and  $15$  K; the dashed-line contours represent the negative values.

Fig. 2 shows the principal large-scale kinematic and spatial properties of the neutral hydrogen distribution in Dwingeloo 1. The global HI profile shown in Fig. 2c was obtained by integrating the individual continuum-subtracted channel maps, giving the HI flux density as a function of radial velocity. The global profile shows the two-horned signature characteristic of an inclined spiral galaxy, with the flux enhanced at the edges of the profile by velocity crowding. The arrow in the global-profile panel indicates the systemic velocity of  $110.3 \pm 0.4$  km s $^{-1}$  as derived from the velocity field of Dw1. The radial velocity of Dw1 with respect to the center of our Galaxy is  $v_G = 110 + 220 \cos(b) \sin(l) = 257$  km s $^{-1}$ , assuming a circular velocity of the LSR of 220 km s $^{-1}$ .

A map of the spatial distribution of the total integrated HI column density in Dw1 is shown in Fig. 2h. This total-HI map was constructed by adding all the channel maps, after having set the pixels outside the defined areas to zero. Because the number of added channels thus varies from pixel to pixel, the noise in the total-HI map varies as well from pixel to pixel, independent of the strength of the signal.

The panels of Fig. 2e show position-velocity diagrams corresponding, respectively, to the major axis of the total-HI map, determined at a position angle of  $112^\circ$ , and to the minor axis of the total-HI map, at a position angle of  $202^\circ$ .

The observed (projected) velocity field of Dw1 shown in Fig. 2g was determined by fitting single Gaussians to each velocity profile through the data cube. Only those Gaussian solutions were accepted which met the three-fold criterion of returning a peak inside the area defining the HI emission, of returning a peak amplitude greater than 3 times the noise in the profile in question, and of yielding a peak velocity with an error less than a third of the velocity resolution of the WSRT data.

The kinematic and spatial characteristics of Dw1 mentioned above are indicative of a well-behaved system. Such behavior justifies further analysis based on a model of tilted, rotating rings. This analysis technique has been described by Begeman (1989). Fig. 2i shows the results of modelling the observed velocity field with such tilted rings. The width of each ring was held constant at value equal to  $2/3$  of the size of the major axis of the synthesized WSRT beam.

The ring fitting involved three steps. First, the systemic velocity, the center of rotation, and the rotation velocity were modelled for each ring keeping the inclina-

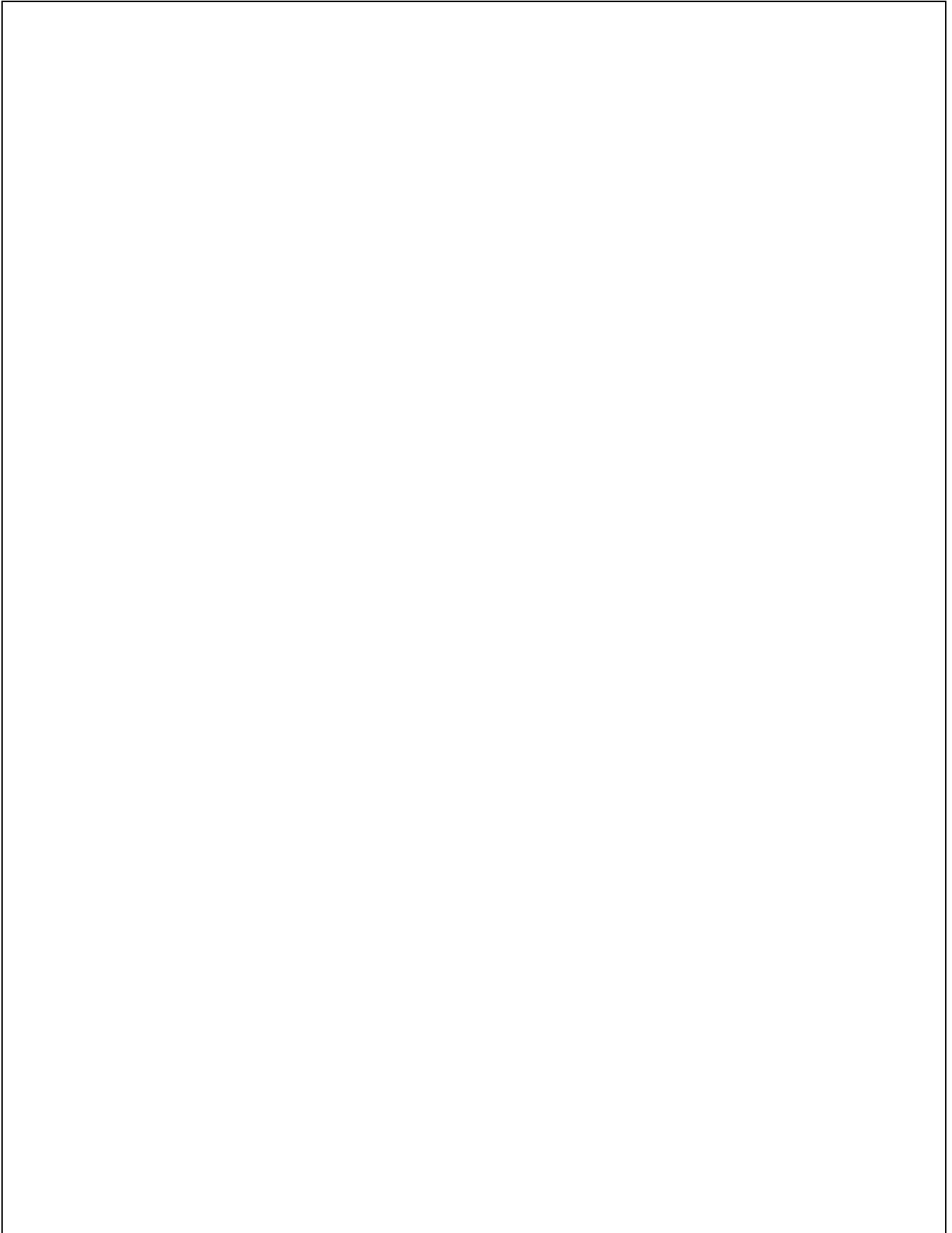
tion and position angle fixed at values derived from fitting ellipses to the total HI map. No significant trend in either systemic velocity or in rotation center as a function of radius was detected; in the subsequent steps, the rings were therefore treated as spatially and kinematically concentric. Second, the rotation velocity, the position angle, and the inclination were fit for each ring keeping the systemic velocity and center fixed at the previously-determined average values. No significant trend of inclination from the mean value of  $51^\circ$  (measured such that an edge-on galaxy is inclined  $90^\circ$ ) was detected as a function of radius which might be taken as indication of a morphological property of the galaxy such as warping; some localized wiggles in the parameters might be due to the influence of spiral structure. A slight change of position angle detected near the center of Dw1 may well be caused by non-circular motion due to the presence of the bar evident on infrared and optical images of the galaxy (see Kraan–Korteweg et al. 1994; Loan et al. 1995). Finally, the rotation velocity and the position angle were fit for each ring, keeping all other parameters fixed. This last step was done in half rings, separately for the receding and for the approaching sides of Dw1, in order to investigate the degree of symmetry of the rotating disk. The substantial symmetry of the system is indicated by the two panels of Fig. 2e, where the mean rotation curve is projected on the position-velocity diagrams.

The orientations of the rings as derived by the tilted-ring model were used to derive a radial HI profile by averaging the HI column density from the total HI map in annuli corresponding to the projected rings. The width of the annuli was set to  $2/3$  of the major axis of the synthesized WSRT beam. Fig. 2d shows the variation of the deprojected HI surface density in solar-mass units with angular distance from the galactic center, plotted separately for the receding and the approaching sides of Dw1. The vertical arrow indicates the angular extent of the semi-major axis of the *I*-band image.

Finally, Fig. 2b shows the 21-cm continuum emission from Dw1. This emission, which is contributed from the entire extended disk, has an integrated flux of  $48.2 \pm 7.5$  mJy and suggests on-going star formation in the galaxy.

#### 4. HI in the newly discovered galaxy Dwingeloo 2

The Westerbork observations resulted in the discovery of a small galaxy, located some 21 arcminutes to the west-northwest of Dw1 and quite likely its companion. The



H I signal from this galaxy, which we call Dwingeloo 2, would have been heavily blended in the single-dish detection spectrum of Dw1. The signals from the two systems are centered less than  $20 \text{ km s}^{-1}$  apart in velocity, and their angular separation is less than the FWHM of the beam of the Dwingeloo 25-m telescope.

We were unable to find Dwingeloo 2 on the POSS I plates, but inspection of the red POSS II plate revealed a feature of low surface brightness, elongated like the WSRT H I image. C. Aspin, and R. Tilanus have detected the stellar component of Dw2 in observations made using the IRCAM3 (see Puxley et al. 1994) camera operating at a wavelength of  $2.2 \mu\text{m}$  on the UKIRT facility on Mauna Kea. They have kindly provided the  $K$ -band image reproduced in Fig. 4a. This image reaches a depth of  $m_K = 20$ ; although the signal from the stellar component of Dw2 is weak, it has evidently been detected as a smudge inclined on the sky in the same manner as the gaseous component and as the POSS II feature. (We note that the possibilities now becoming available of deep imaging at  $2.2 \mu\text{m}$ , as well as of surveying at this wavelength, will likely lead to upward revisions of the sizes and stellar masses of heavily obscured galaxies, as well as to the discovery of additional ones.)

Fig. 3 is a mosaic showing the H I emission from Dw2 in individual channel maps, each centered at the indicated velocity. Despite the decreased sensitivity (40% of maximum) of the primary beam at the off-axis position of Dw2, the small galaxy contributes easily-detected signals to the panels between  $32$  and  $155 \text{ km s}^{-1}$ . The “spider-diagram” signature so pronounced in Dw1 does not characterize the Dw2 channel maps: the H I disk of Dw2 apparently rotates as a solid body. We note, however, that the H I distribution in each channel map is not quite perpendicular to the overall kinematic major axis as would be expected for an unperturbed disk rotating as a solid body.

Fig. 4 shows the principal kinematic and spatial global properties of the H I distribution in Dw2; these properties were extracted from the WSRT data in the same manner as described for Dw1. The global H I profile shown in Fig. 4c does not show the two-horned signature, because of the absence of the velocity-crowding which would follow from an extensive region spanned by an essentially flat rotation curve. The systemic velocity of Dw2 as derived from the velocity field is  $94.0 \pm 1.5 \text{ km s}^{-1}$  and is indicated by the arrow in the global-profile panel. The radial velocity of Dw2 with respect to the center of our Galaxy is  $v_G = 94 + 220 \cos(b) \sin(l) = 241 \text{ km s}^{-1}$ .

A map of the spatial distribution of the total integrated H I column density in Dw2 is shown in Fig. 4h. The total-H I distribution is rather irregular and thus poorly suited to estimating the inclination of Dw2.

The projected velocity field shown in Fig. 4g was determined by fitting single Gaussians to each velocity profile through the data cube, in a procedure identical to that followed for the Dw1 data. The observed velocity field

**Table 2.** Rotation curves (deprojected for inclination) for Dwingeloo 1 and Dwingeloo 2, derived from least-squares modelling of concentric, rotating, tilted rings

Dwingeloo 1			Dwingeloo 2	
R ( $''$ )	$v_{\text{rot}}$ ( $\text{km s}^{-1}$ )	P.A. ( $^\circ$ )	$v_{\text{rot}}$ ( $\text{km s}^{-1}$ )	P.A. ( $^\circ$ )
20	$20.9 \pm 1.6$	$135.2 \pm 5.5$	$19.5 \pm 2.6$	$296.7 \pm 6.0$
40	$42.3 \pm 1.1$	$127.3 \pm 2.1$	$28.4 \pm 1.2$	$297.9 \pm 2.4$
60	$67.8 \pm 1.0$	$115.4 \pm 1.1$	$33.5 \pm 1.3$	$291.4 \pm 1.9$
80	$83.8 \pm 0.7$	$114.3 \pm 0.6$	$37.9 \pm 1.8$	$281.8 \pm 2.7$
100	$90.9 \pm 0.6$	$112.0 \pm 0.5$	$43.5 \pm 0.9$	$274.8 \pm 1.3$
120	$94.1 \pm 0.5$	$111.3 \pm 0.4$	$48.0 \pm 0.9$	$269.5 \pm 1.1$
140	$97.9 \pm 0.5$	$113.2 \pm 0.4$	$51.6 \pm 1.0$	$271.4 \pm 1.1$
160	$101.6 \pm 0.4$	$114.2 \pm 0.3$		
180	$104.9 \pm 0.5$	$113.8 \pm 0.4$		
200	$108.3 \pm 0.5$	$113.0 \pm 0.4$		
220	$110.7 \pm 0.4$	$112.4 \pm 0.3$		
240	$112.4 \pm 0.4$	$111.9 \pm 0.3$		
260	$113.5 \pm 0.4$	$111.6 \pm 0.3$		
280	$113.6 \pm 0.4$	$111.8 \pm 0.3$		
300	$112.7 \pm 0.5$	$112.3 \pm 0.3$		
320	$113.9 \pm 0.5$	$113.0 \pm 0.3$		
340	$115.4 \pm 0.4$	$112.4 \pm 0.3$		
360	$114.2 \pm 0.5$	$111.7 \pm 0.3$		
380	$112.3 \pm 0.5$	$112.0 \pm 0.3$		
400	$110.6 \pm 0.6$	$111.2 \pm 0.4$		
420	$110.2 \pm 0.6$	$112.0 \pm 0.4$		
440	$109.0 \pm 1.1$	$114.9 \pm 1.0$		

seems to be twisted, suggesting a dominant central bar or a warp in the outer regions. Modeling the velocity field of Dw2 by tilted concentric rings, assuming circular motions and thus ignoring a possible bar potential, shows a rather constant inclination angle of  $69^\circ$  but a clear change in position angle from  $294^\circ$  in the inner regions to  $271^\circ$  in the outer ones. The results of the tilted-ring fit are shown in the three panels of Fig. 4f. Note that the kinematic position angles do not reflect the position angle of the overall H I distribution; this situation favors the idea of a bar potential over that of a warp.

The left-hand panel of Fig. 4e shows a position-velocity diagram at the position angle of the kinematic major axis in the inner region of Dw2; the right-hand panel shows the position-velocity slice along the kinematic minor axis in the inner region. Both diagrams are centered on the derived dynamical center of Dw2. The dots represent the rotation curve projected on to these slices.

Fig. 4d shows the deprojected H I surface density, in units of  $M_\odot \text{ pc}^{-2}$ , plotted separately for the approaching and receding sides of Dw2. The integrations were done in ellipses prescribed by the results from the tilted-ring modelling. Although the central H I surface densities in Dw 1 and in Dw2 are quite similar, the densities in Dw2 fall rapidly with distance from its center.

**Fig. 4.** Global kinematic and spatial properties of the H I distribution in Dwingeloo 2. Panel *a*) shows, for comparison with the global H I situation, a greyscale representation of the UKIRT *K*-band image kindly provided by R. Tilanus and C. Aspin. Panel *b*) shows the *CLEAN*ed continuum map, with contours drawn at levels of  $-1.2$ ,  $-0.58$ ,  $0.58$  (the  $2\text{-}\sigma$  level),  $1.2$ ,  $2.3$ ,  $4.6$ ,  $9.3$ , and  $19$  K. Panel *c*) shows the global H I line profile in mJy, corrected for the sensitivity of the primary beam; the vertical arrow shows the systemic velocity of Dw2,  $94.0$  km s $^{-1}$ , as derived from the velocity-field data. Panel *d*) shows the deprojected H I surface density in units of  $M_{\odot}$  pc $^{-2}$ , as determined in tilted rings separately for the approaching and receding sides of Dw2; the full-drawn line corresponds to the average of the surface densities measured on the two sides. The panels labelled *e*) show position-velocity maps of the H I emission observed, at the indicated position angles, along the major axis (left) and along the minor axis (right) of Dw2. Contours in the major-axis position-velocity map correspond to  $-0.21$ ,  $0.21$  (the  $2\text{-}\sigma$  level),  $0.42$ , and  $0.85 \times 10^{20}$  H I atoms cm $^{-2}$ ; in the minor-axis map, the contours correspond to  $-0.20$ ,  $0.20$  ( $2\sigma$ ),  $0.40$ ,  $0.81$ , and  $1.2 \times 10^{20}$  H I atoms cm $^{-2}$ . The dots follow the rotation curve as projected onto this position-velocity maps. In both panels, the horizontal dashed line gives the systemic velocity while the vertical one corresponds to the location of the center of rotation. The cross in the lower-lefthand corner of each of the position-velocity slices gives the spatial and kinematic resolution of the WSRT data on Dw2. Panel *g*) shows the observed velocity field determined for Dw2 by Gaussian fitting to individual H I spectra. The lighter greyscale and the black contours correspond to the approaching side; the darker greyscale and the white contours, to the receding. The heavily-drawn black contour follows the systemic velocity. The interval between contour lines is  $15$  km s $^{-1}$ , measured from the systemic velocity of  $94.0$  km s $^{-1}$ . Panel *i*) shows the modelled velocity field as a “spider diagram” derived by fitting the observed field with tilted rings in which the H I describes circular rotation; the isovelocity contours in this panel are drawn as in *g*). Panel *j*) shows the difference between the observed and modelled velocity fields; the contours give the velocity residuals at levels of  $-10$ ,  $-5$ ,  $5$ , and  $10$  km s $^{-1}$ . Panel *h*) shows the distribution of the total H I column density across Dw2. As indicated in the text, the noise level varies across this map. Greyscaled pixels in the total-H I map all have a signal-to-noise ratio  $\geq 1.5$ ; the contours correspond to  $1.3$  (mean  $S/N = 3$ ),  $2.2$ ,  $4.2$ ,  $6.3$ ,  $8.4$ , and  $13 \times 10^{20}$  H I atoms cm $^{-2}$ . The three panels in *f*) show the radial variations of, respectively beginning with the upper of the three, the inclination of tilted rings fit to Dw2, the position angle of these rings, and the rotation velocity. The shaded circle in the lower left of the two upper panels and in the lowermost left-hand panel indicates the FWHM of the synthesized WSRT beam.

## 5. Concluding remarks on the intrinsic properties of Dwingeloo 1 and Dwingeloo 2

Figs. 5 and 6 place Dw1 and Dw2 together in their relative position and orientation on the sky, with Fig. 5 showing the total H I maps for the two galaxies and Fig. 6 their velocity fields.

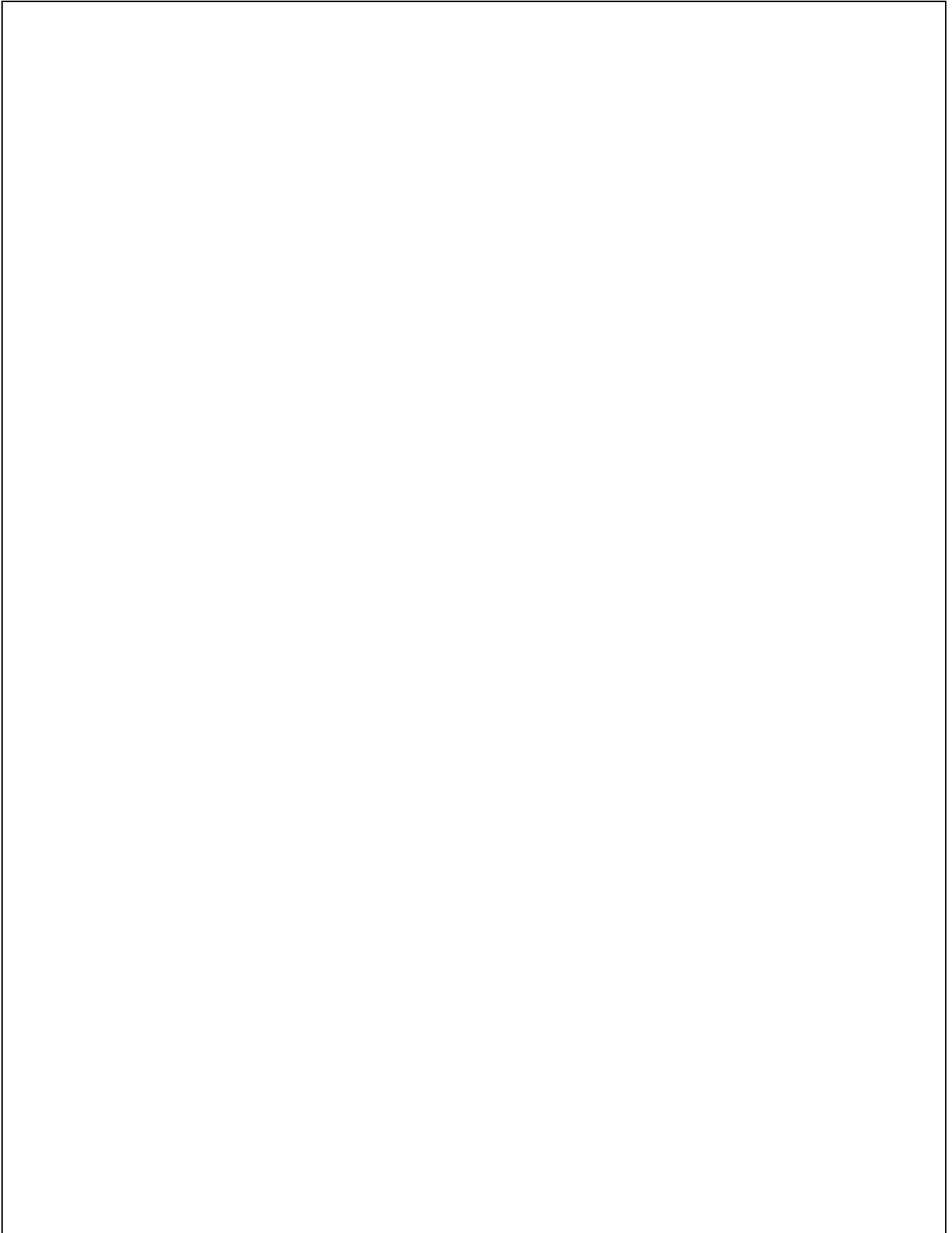
The assignment of Dw1 to the class of barred spiral galaxies is most clearly required by the appearance of the UKIRT *K*-band image obtained on August 10, 1994, by R. Tilanus, C. Aspin, and T. Geballe. (This image was printed in the IAU General Assembly Newsletter “Sidereal Times”, #3, August 18, 1994.) The *K*-band data show the unmistakable signature of a bar, oriented along the major axis of the H I distribution as determined from the WSRT data, and extending to about 1.5 arcminutes from the center of the galaxy. The INT and Wise Observatory *I*-band images confirm this assignment (see Loan et al. 1995). Both the *K*- and *I*-band images show spiral arms emanating from the ends of the stellar bar, and winding over some  $180^{\circ}$  in azimuth. The superposition shown in Fig. 7 of the WSRT total-H I map overlaid on the *I*-band image shows that the optically-traced structure is continued to larger radii in the H I distribution. The residual velocity-field map shown in Fig. 2j suggests that the spiral structure at larger radii perturbs the kinematics of Dw1 in a manner not uncommon for such galaxies. The plot of H I surface density against distance from the center shown in Fig. 2d shows a relative deficiency of H I emission from the region of Dw1 occupied by the stellar bar; such morphology is also not uncommon.

Dw1 displays a quite simple morphology. There is no indication of a substantial lopsidedness in the H I surface distribution, nor is there any compelling indication of the kinematic or spatial distortions which would be expected if the galaxy was severely warped, or if it were undergoing an interaction with a close-by neighboring system of comparable or higher mass.

Dw2 is located approximately along the extension of the major axis of Dw1. Unlike the simplicity pertaining for the larger galaxy, the kinematic and spatial properties of Dw2 do suggest that this smaller system might be distorted by an interaction with the more massive Dw1. The isovelocity contours shown in Fig. 6 and in Fig. 4g show a twist which might be associated with a gravitational distortion of the smaller system by the larger one. The panels in Fig. 4f showing the variation of inclination and of position angle of the fitted tilted rings additionally suggest a distortion of Dw2. (The panels in Fig. 2f showing the same information for Dw1 indicate no significant variation of inclination or of position angle over distance from the center of Dw1.)

Table 2 gives the rotation curves for Dwingeloo 1 and Dwingeloo 2, as derived from least-squares modelling of the observed velocity fields by concentric, rotating, tilted rings; the values tabulated have been corrected for the inclinations of the galaxies. We note that the H I surface density of Dw2 drops below detectability in the outer regions before reaching a regime of flat rotation.

The suggested distortion of Dw2 by Dw1 remains tentative until the linear distance between the two systems



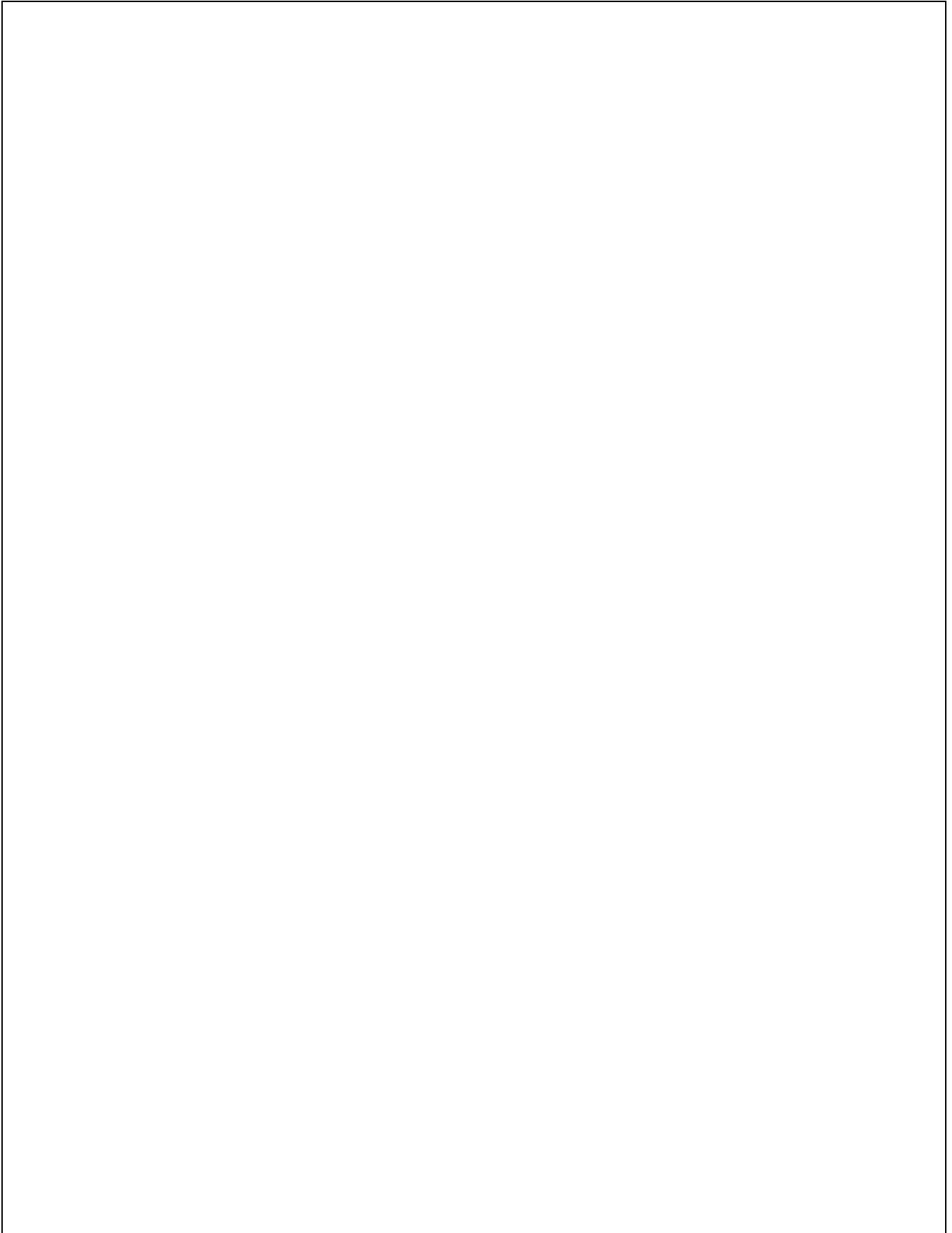


**Fig. 5.** Distribution on the sky of H I column densities measured in Dwingeloo 1 and Dwingeloo 2. The column densities are given by the false-color coding as indicated by the color bar on the right-hand side of the figure. The circle in the lower-left-hand corner represents the FWHM of the synthesized WSRT beam. Dw2 is located at an angular separation from Dw1 of some  $21'$ , approximately along an extension of the major axis of Dw1. If the two galaxies are located at the same distance from the Sun, and if this distance is 3.8 Mpc (see Loan et al. 1995; cf. Kraan–Korteweg et al. 1994), then the angular separation corresponds to a linear distance of 24 kpc.

**Fig. 6.** Velocity fields revealed by H I observations of Dwingeloo 1 and Dwingeloo 2. The velocities are given by the false-color coding as indicated by the color bar on the right-hand side of the figure. The circle in the lower-left-hand corner represents the FWHM of the synthesized WSRT beam. Dw2 is located near the extended major axis of Dw1. There is some indication of a kinematic distortion in the smaller system which tentatively suggests that Dw2 is a companion to Dw1.

**Table 3.** Intrinsic properties of Dwingeloo 1 and Dwingeloo 2 derived from the WSRT observations

		Dwingeloo 1	Dwingeloo 2
dynamical center (eq. coord.)	$\alpha_{1950}$	$02^h 53^m 01^s.6$	$02^h 50^m 21^s.7$
	$\delta_{1950}$	$58^d 42' 43''$	$58^d 48' 07''$
dynamical center (gal. coord.)	$l$	$138^\circ 52$	$138^\circ 17$
	$b$	$-0^\circ 11$	$-0^\circ 19$
integrated HI flux	(Jy km s $^{-1}$ )	$205.2 \pm 1.2$	$30.8 \pm 0.5$
HI profile widths, 20%	(km s $^{-1}$ )	$201.2 \pm 0.4$	$116.6 \pm 1.6$
50%	(km s $^{-1}$ )	$187.6 \pm 0.6$	$99.9 \pm 1.2$
systemic velocity ( $LSR$ )	(km s $^{-1}$ )	$110.3 \pm 0.4$	$94.0 \pm 1.5$
diameter of HI disk	(arcmin)	13.7	6.4
continuum flux at $\lambda 21\text{cm}$	(mJy)	$48.2 \pm 7.5$	$< 16^1$
inclination	(degrees)	$51 \pm 2$	$69 \pm 3$

<sup>1</sup> $3\text{-}\sigma$  limit for extended continuum emission from Dw2

is better known. The matter of the distance to the two galaxies is, of course, important in several regards. It is not reasonable to use the Hubble-flow to gauge the distance to such nearby systems. Instead, Kraan–Korteweg et al. (1994) estimated the distance to Dw1 at about 3 Mpc on the basis of the blue Tully–Fisher relationship between the extinction-corrected absolute magnitude and the inclination-corrected H I linewidth. The galactic extinction was determined by Kraan–Korteweg et al. following the precepts of Burstein & Heiles (1982) and using the H I column density determined from the data of the Leiden/Dwingeloo survey of Hartmann & Burton (1995). The principal uncertainties in this estimate stem from the large scatter in the blue Tully–Fisher relationship and in the unprecedented use of the Burstein–Heiles relationship at the high values of  $N_{\text{HI}}$  found near to  $b = 0^\circ$ . It is not at all ruled out that the Galactic H I spectra so close to the equator are partially saturated (see Burton, 1993), and if saturation does cause the extinction derived from the integrated H I to be underestimated, then the distance of 3 Mpc may also be underestimated. Loan et al. (1995) derived the distance to Dw1 using the  $I$ - and  $R$ -band versions of the Tully–Fisher relation; this has the advantage that corrections for Galactic and internal extinctions are smaller in the near infrared than in the blue. Loan et al. choose as the most likely distance for Dw1 the value 300

km s $^{-1}$ , although they stress that the distance uncertainties remain substantial. Assuming that the value of the Hubble constant is  $80 \text{ km s}^{-1} \text{ Mpc}^{-1}$ , we are led to adopt the value of 3.8 Mpc as the distance to Dw1 in order to proceed with estimating characteristic physical aspects of the galaxies.

If Dw1 is at a distance of 3.8 Mpc then its H I angular diameter corresponds to a linear size of 15 kpc. This estimate of the H I diameter may be compared with the dimension of the  $K$ -band bar as projected at 3.8 Mpc distance, namely about 2.5 kpc, and with the dimension of the IRAS 60- $\mu\text{m}$  image (see Loan et al. 1995), namely about 4 kpc. The flat regime of the H I rotation curve pertains beyond about 4 kpc. If Dw2 is at the same distance as Dw1, its H I diameter is 7 kpc. The projected angular distance between Dw1 and Dw2 corresponds to a lower-limit on their linear separation of only 24 kpc.

The total H I mass harbored by the galaxies follows from  $2.36 \times 10^5 D^2 I_{\text{HI}}$ , where  $D$  is the distance in Mpc and  $I_{\text{HI}}$  is the integrated H I flux. For Dw1,  $M_{\text{HI}} = 7.0 \times 10^8 M_\odot$ ; for Dw2,  $M_{\text{HI}} = 1.1 \times 10^8 M_\odot$ .

The above values for the H I and near- and far-infrared-image diameters as well as for the H I mass of Dw1 are consistent with what would characterize a modest barred spiral galaxy; the values for Dw2 also seem plausible for the small companion. The total mass (i.e. including stel-

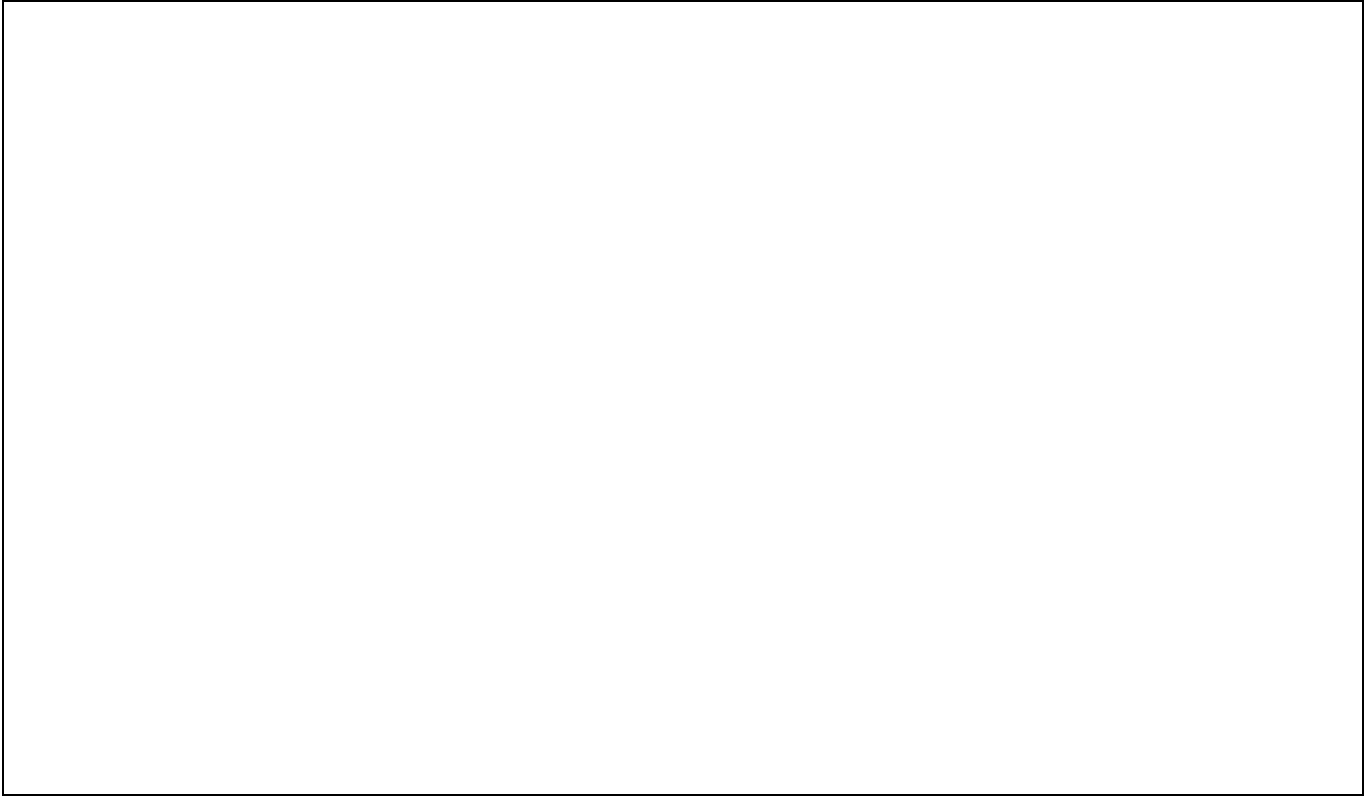




**Fig. 7.** Superposition of the WSRT map of the Dw1 H I surface densities, shown by contours, on the *I*-band false-color image from the INT (Loan et al. 1995). The H I surface density contours are drawn at the same levels as those in Fig. 2b; regions of highest density are encircled by the red contour. The circle in the lower-left hand corner represents the FWHM of the synthesized WSRT beam.

lar as well as any dark matter) within a radius  $r$  can be estimated from  $M_{tot}(< r) = (v_{rot})^2 r / G$ , where  $v_{rot}$  is the deprojected rotation speed. For Dw1,  $v_{rot}$  is about 113 km s<sup>-1</sup>. Taking  $r$  as the distance of the last measured point on the rotation curve (see Table 2), namely at about 7'5 for Dw1 or at about 2'5 for Dw2, then the total mass to this distance in Dw1 follows at the value  $3.1 \times 10^{10} M_{\odot}$  for Dw1 and at the value  $2.3 \times 10^9 M_{\odot}$  for Dw2. The ratio  $M_{HI}/M_{tot}$  would be about 0.02 for Dw1 and about 0.05 for Dw2; these values seem plausible for a spiral and for a gas-rich dwarf, respectively.

It is interesting to compare the total mass of Dw1 with that of the Milky Way as well as with that of Dw2; this comparison follows simply from the squared ratio of ro-

tation speeds in the outer flat-rotation regimes, which is  $M_{MW}/M_{Dw1} = (220/113)^2 = 3.8$  for the ratio of total mass of the Milky Way compared to Dw1. For Dw2, where HI has not been detected from a flat-rotation regime, we take  $v_{rot}$  at the maximum measured value of about 52 km s<sup>-1</sup>. This value then yields a rough estimate of the ratio of  $M_{Dw1}/M_{Dw2} \sim (113/52)^2 = 4.7$  for the Dw1/Dw2 comparison of total masses. These ratios give reasonable estimates of the relative masses within the relevant radii, but do not give accurate estimates of the relative *total* masses, because the true total extents are not yet known. At the presumed distance and with the total mass estimated as indicated, the mass of Dw1 would be comparable to that of M33.



**Fig. 8.** Superposition of the WSRT map of the Dw2 H I surface densities, shown by contours, on the  $K$ -band false-color image from the UKIRT IRCAM3 image kindly provided by R. Tilanus and C. Aspin. The H I surface density contours are drawn at the same levels as those in Fig. 4b; regions of highest density are encircled by the red contour. The circle in the lower-left hand corner represents the FWHM of the synthesized WSRT beam.

The distance estimate of 3.8 Mpc and the angular proximity of Dw1 & 2 to the galaxies Maffei 1 & 2 and IC342, make the conclusion plausible that these galaxies are all members of the same grouping. Recently McCall & Buta (1995) discovered two dwarf companions to Maffei 1; although these dwarfs would probably contribute little to the overall mass budget of the group, their discovery additionally motivates searches for galaxies in the vicinity. We note that before the detection of Dw1 there were several predictions, for different reasons, concerning the likelihood of an undetected galaxy near Maffei 1 and 2. Hurt et al. (1993) pointed out a number of morphological distortions and other features evident in a deep  $K$ -band image of Maffei 2 that were taken as indications of a recent

interaction with a companion galaxy. Peebles (1990) concluded that the motions of the Maffei group suggested the presence of a nearby galaxy, as then undetected. Whether or not the two Dwingeloo galaxies exercise any significant dynamical influence on the motions of the Maffei/IC342 group remains a matter for further consideration.

*Acknowledgements.* The Westerbork Synthesis Radio Telescope and the Dwingeloo 25-meter telescope are operated by the Netherlands Foundation Research in Astronomy with support from the Netherlands Organization for Scientific Research (NWO). While in Groningen the research of R.C.K.-K. was made possible by a fellowship from the Royal Netherlands Academy of Arts and Sciences. We are grateful to D. Moorrees for continuing assistance with the Dwingeloo Obscured Galax-

ies Survey observing program on the 25-m telescope, and to A. Foley, H. Kahlmann, and T. Spoelstra for the rapid scheduling and initial calibration of the WSRT observations. We are grateful to R. Tilanus and C. Aspin for providing the UKIRT *K*-band image of Dw2.

## References

- Begeman K.G., 1989, *A&A* 223, 47
- Burstein D., Heiles C., 1982, *AJ* 86, 1165
- Burton W.B., 1993, Distribution and Observational Properties of the ISM. In: Pfenniger D., Bartholdi P. (eds.) *The Galactic Interstellar Medium*. Springer-Verlag, Heidelberg, p. 1
- Burton W.B., Hartmann D., 1994, The Leiden/Dwingeloo Survey of H I in our Galaxy. In: Balkowski C., Kraan-Korteweg R.C. (eds.) *Unveiling Large-Scale Structures Behind the Milky Way*. ASP Conference Series 67, p. 31
- Hartmann D., 1994, Ph.D. Thesis, University of Leiden
- Hartmann D., Burton W.B., 1995, *Atlas of Galactic Neutral Hydrogen*. Cambridge University Press, Cambridge (under contract)
- Hau G.K.T., Lahav O., Ferguson H.C., Lynden-Bell D., 1995, *MNRAS* (in press)
- Henning P.A., 1992, *ApJS* 78, 365
- Henning P.A., 1994, Searching at 21 cm for Galaxies in the Zone of Avoidance. In: Balkowski C., Kraan-Korteweg R.C. (eds.) *Unveiling Large-Scale Structures Behind the Milky Way*. ASP Conference Series 67, p. 203
- Högbom J.A., 1974, *A&AS* 15, 417
- Huchtmeier W.K., Lercher G., Seeberger G., Sauer W., Weinberger R., 1995, *A&A* 293, 33
- Hurt R.L., Merrill K.M., Gatley I., Turner J.L., 1993, *AJ* 105, 121
- Kerr F.J., 1994, The Early History of Galaxy Searches in the ZOA. In: Balkowski C., Kraan-Korteweg R.C. (eds.) *Unveiling Large-Scale Structures Behind the Milky Way*. ASP Conference Series 67, p. 3
- Kerr F.J., Henning P.A., 1987, *ApJ* 320, L99
- Kraan-Korteweg R.C., Loan A.J., Burton W.B., Lahav O., Ferguson H.C., Henning P.A., Lynden-Bell D., 1994, *Nat* 372, 77
- Kraan-Korteweg R.C., Loan A.J., Burton W.B., Lahav O., Ferguson H.C., Henning P.A., Lynden-Bell D., 1995, *Astro. Lett. and Communications* 31, 227
- Kraan-Korteweg R.C., Woudt P.A., 1994, An Optical Galaxy Search in the Hydra/Antlia and the Great Attractor Region. In: Balkowski C., Kraan-Korteweg R.C. (eds.) *Unveiling Large-Scale Structures Behind the Milky Way*. ASP Conference Series 67, p. 89
- Loan A.J., Maddox S.J., Lahav O., Balcells M., Kraan-Korteweg R.C., Assendorp, R., Amoznino E., Brosch N., Goldberg E., Ofek E.O., 1995, *MNRAS* (submitted)
- Lockman F.J., 1989, *ApJS* 71, 469
- McCall M.L., Buta R.J., 1995, *AJ* 109, 2460
- Peebles P.J.E., 1990, *ApJ* 362, 1
- Puxley P.J., Sylvester J., Pickup D.A., et al., 1994, *SPIE* 2198
- Van Someren Greve H.W., 1974, *A&AS* 15, 343
- Verheijen M.A.W., 1996, Ph.D. Thesis, University of Groningen